Reduced Graphene Oxide Thin Films as Ultrabarriers for Organic Electronics

Hisato Yamaguchi, Jimmy Granstrom, Wanyi Nie, Hossein Sojoudi, Takeshi Fujita, Damien Voiry, Mingwei Chen, Gautam Gupta, Aditya D. Mohite, Samuel Graham, and Manish Chhowalla**

Encapsulation of electronic devices based on organic materials that are prone to degradation even under normal atmospheric conditions with hermetic barriers is crucial for increasing their lifetime. A challenge is to develop ultrabarriers that are impermeable, flexible, and preferably transparent. Another important requirement is that they must be compatible with organic electronics fabrication schemes (i.e., must be solution processable, deposited at room temperature and be chemically inert). Here, a lifetime increase of 1300 h for poly(3-hexylthiophene) (P3HT) films encapsulated by uniform and continuous thin (≈10 nm) films of reduced graphene oxide (rGO) is reported. This level of protection against oxygen/water vapor diffusion is substantially better than conventional polymeric barriers such as Cytop, which degrades after only 350 h despite being 400 nm thick. Analysis using atomic force microscopy, X-ray photoelectron spectroscopy, and high-resolution transmission electron microscopy suggest that the superior oxygen gas/moisture barrier property of rGO is due to the close interlayer distance packing and absence of pinholes within the impermeable sheets. These material properties can be correlated to the enhanced lag time of 500 h. The results provide new insight for the design of high-performance and solution-processable transparent ultrabarriers for a wide range of encapsulation applications.

1. Introduction

The performance of organic-inorganic multilayer ultrabarriers for encapsulation of organic and other environmentally sensitive electronics is limited by unavoidable pinholes in the inorganic layer (typically AlO_x and SiO_x) during vacuum deposition.[1–3] Increasing the thickness of the inorganic film can mitigate this limitation but introduces new defects, i.e., cracks induced by stress in the films. State of the art barriers consist of repeated stacking of organic-inorganic units, referred to as "dyad" structure to increase the diffusion length of the gas species.[1,4] However, this is problematic due to the increased fabrication complexity as well as loss of flexibility. Furthermore, elimination of the vacuum deposition step for ultrabarriers would be beneficial for device fabrication methods such as roll-to-roll processing. Therefore it is desirable to fabricate impermeable, flexible, and preferably transparent ultrabarriers via solution processing that is free from complexity of the stacked dyad structure.

Graphene is an atomically thin sheet of carbon, which possesses attractive material properties, especially as ultrabarrier layers.[5–8] Its closely packed hexagonal atomic structure prevents permeation of even hydrogen,[9] and being atomically thin makes it flexible and optically transparent. Mechanical exfoliation and chemical vapor deposition (CVD) are known routes to obtain less defective graphene but uniform deposition over large areas on arbitrary substrates at low temperatures may limit their use as barriers.[10–12] We have therefore investigated the barrier properties of graphene oxide (GO) obtained from chemical exfoliation of graphite.[13–15] GO consists of atomically thin sheets of graphene that are decorated with oxygen functional groups and has microscopic lateral dimensions.[16] It is well known that in contrast with pristine graphene, GO is highly defective and chemically heterogeneous. It can be made electrically active by evolving oxygen from its structure but these can introduce holes in the basal plane of the GO sheets.[17] Continuous layers of GO and rGO can be deposited using several techniques[18–20] but it is unclear if impermeability can be introduced in such thin films. Here we demonstrate that GO and rGO layers exhibit excellent hermeticity, and the presence of

Dr. H. Yamaguchi, Dr. D. Voiry, Prof. M. Chhowalla
Department of Materials Science and Engineering
Rutgers University
607 Taylor Road, Piscataway, NJ, 08854, USA
E-mail: manish1@rci.rutgers.edu
Dr. H. Yamaguchi, Dr. W. Nie, Dr. G. Gupta, Dr. A. D. Mohite
Center for Integrated Nanotechnologies (CINT)
Materials Physics and Applications (MPA) Division
Mail Stop: K771, Los Alamos National Laboratory (LANL)
P.O. Box 1663, Los Alamos, NM, 87545, USA
E-mail: hisatoy@lanl.gov
Dr. J. Granstrom, Dr. H. Sojoudi,[+] Prof. S. Graham
Center for Organic Photonics and Electronics and Woodruff School of Mechanical Engineering
Georgia Institute of Technology, Atlanta, GA, 30332, USA
Prof. T. Fujita, Prof. M. Chen
WPI Advanced Institute for Materials Research
Tohoku University, 2–1–1 Katahira
Aoba-ku, Sendai, Miyagi, 980–8577, Japan
[+]Present address: Department of Chemical Engineering, Massachusetts Institute of Technology, 77 Massachusetts Avenue, Cambridge, MA 02139, USA

DOI: 10.1002/aenm.201300986

oxygen functional groups attached to both sides of the graphene basal plane can act as atomically thin organic layers of the dyad structure. Although some efforts have already been made to use solution processed and transparent GO as hermetic films, reports generally focus on its incorporation in polymer composites, where GO serves merely as impermeable sheets that are randomly oriented and widely spaced.[21,22] These types of structures create permeation paths in the films, limiting the contribution of barrier effects from the GO. Recently, Yang et al.[23] reported significantly enhanced gas barrier performance using well-ordered GO film-polymer bilayer. However, evaluation of intrinsic gas barrier properties of GO and rGO thin films remain unexplored. The elucidation of their gas barrier properties including the oxygen diffusion dynamics should allow the design of high performance and solution processable transparent ultrabarriers based on 2D nanosheets.

2. Results and Discussion

We have monitored the degradation of a common electrically active organic material, poly(3-hexylthiophene) (P3HT), to test the barrier properties of GO and rGO. It has been shown that photo-oxidative degradation of P3HT occurs upon exposure to O_2 (also moisture) under illumination, resulting in an increase in the optical transparency.[24] Therefore, monitoring the transparency of the P3HT under humid conditions is a simple and accurate method for determining the barrier properties of GO/rGO thin films. Specifically, photolysis (film degradation due to light exposure in an inert atmosphere) of P3HT occurs at a rate that is several orders of magnitude lower than photo-oxidation for the first few thousand hours of light exposure, thus sufficiently long term oxygen barrier test can be performed using this method.[25] The measurements were made in ambient environment with weak illumination intensity. Illumination was kept low to eliminate possible temperature increase of the samples as well as reduction of GO by light (see Experimental Section for details).[26] In addition to GO and rGO layers, control measurements were also made on P3HT alone and Cytop covered P3HT. Cytop is a highly transparent amorphous fluoropolymer, which was chosen based on its high gas barrier property that exhibits up to an order of magnitude lower water vapor transmission rate than other polymer barriers, e.g. polyvinylacetate (PVAc) and polymethylmethacrylate (PMMA).[27]

Figure 1a shows the normalized transmittance of P3HT films versus time for different barrier films (after subtracting transmittance of the barrier material). Thin (10 nm) and thick (20 nm) films of GO along with 15 nm rGO films (prepared by reducing thick (20 nm) GO films) were prepared by vacuum filtration for evaluation. The inset in Figure 1a shows GO thin films on glass substrate (left), and P3HT encapsulated with thin GO film (right) that are optically transparent. GO films in this thickness range are also flexible as demonstrated in our previous study.[28] Entire P3HT film including the edges was fully encapsulated with GO films (Figure 1b). The summary of degradation as a function of time for each film is plotted in **Figure 2**a (black). As expected, fastest degradation was observed for the bare P3HT film. The transmittance of P3HT showed steady increase, which reached 100% after only 144 h (defined

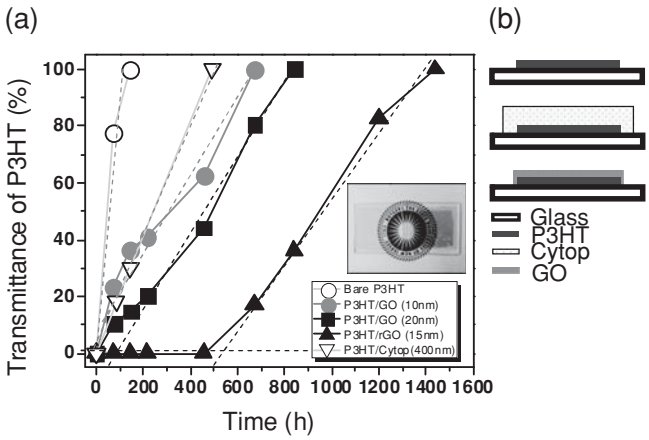

Figure 1. Gas barrier property of GO/rGO films measured by P3HT transmittance test. a) P3HT films on glass substrates were encapsulated with GO and rGO, and compared with controls. The inset shows a photograph of the GO films used for encapsulation on glass (left), and GO encapsulated P3HT films demonstrating high optical transparency of GO films used in this study (right). Dashed line fits used to extract the slope values for calculation of diffusivity in the steady-state flux regime are also shown. b) Schematic of sample structures used for the P3HT transmittance tests.

as lifetime hereafter). The lifetime after encapsulation with 400 nm thick Cytop improved to 493.2 h, a factor of 3.4 increase compared to bare P3HT. This degree of protection against oxygen and water vapor diffusion is consistent with value for Cytop,[29] indicating the validity of the P3HT test for evaluation of oxygen/moisture barrier property. When the P3HT was encapsulated with GO film, however, the lifetime reached 672 h with a film thickness of only 10 nm. The capability of GO films to act as an oxygen barrier with thickness of 10 nm is in sharp contrast to polymer chain-based barrier films including Cytop, which usually require at least 100 nm of thickness to minimize the influence of pinholes.[27] The lifetime can be further improved by simply increasing the film thickness. Increasing the GO film thickness by a factor of 2 (10 nm to 20 nm) leads to an increase in lifetime of up to ≈840 h. The oxygen barrier properties improved substantially after annealing the GO films at 150 °C. The lifetime of rGO barriers reached ≈1440 h, almost ≈800 h improvement compared to non-annealed film with the same number of stacked layers, and 1300 h increase compared to 400 nm thick Cytop film. The rGO film with this superior gas barrier property had an optical transmittance of 75% at 550 nm. Moreover, unlike the other tested barrier films, no increase in the transmittance of the P3HT film was observed in the initial 500 h with rGO barrier films.

To compare the gas barrier properties of the different encapsulation materials, the lifetime was divided by the film thickness to obtain lifetime per unit thickness as summarized in Figure 2a (gray). The obtained values were 1.2 h nm^{-1} for Cytop and 67.2 h nm^{-1} for GO thin film, equating to a factor of ≈50 improvement. The non-linearity in the GO film properties with thickness can be attributed to the fact that the thicker films contain a substantial amount of wrinkles that introduce structural inhomogeneity (Supporting Information, Figure S3).[18] These wrinkles can be "ironed" out via annealing. For rGO film, the lifetime per unit thickness increases substantially up to ≈100 h nm^{-1},

Adv. Energy Mater. 2013,
DOI: 10.1002/aenm.201300986

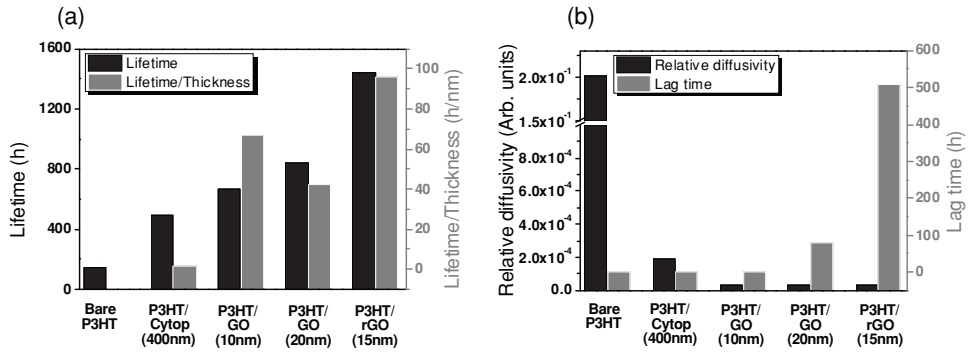

Figure 2. Lifetime values of encapsulated P3HT films. a) Lifetime values extracted from P3HT transmittance test shown for the various different barrier layers tested in this study. Black bars show the total lifetime in hours (left), and gray bars show the lifetime per encapsulated film thickness in h nm^{-1} (right). b) Permeation values showing the relative diffusivity of oxygen (black bars) and lag time for oxygen diffusion to occur (gray bars).

almost double that of GO with same number of stacked layers, and two orders of magnitudes larger than the Cytop.

To gain insight into the gas diffusion dynamics and the origin of improved barrier property of GO/rGO thin films, further analysis of the P3HT transmittance test results was performed. Specifically we focused on two regions: the transition phase in which steady state gas diffusion has not been reached, resulting in very small or no observable permeation; and the steady-state regime where diffusion has reached equilibrium, giving a constant flux of gas species permeating through the barrier films (Supporting Information, Figure S1).[1] The analysis allows determination of the dominant phase in the permeation process, as well as the contribution of each region, which provides information on the barrier dynamics and possible mechanisms. The flux of steady-state phase can be obtained from the slope of the gas barrier lifetime test as shown by the dashed line in Figure 1b. Analysis of the slopes shows very similar values for all of GO/rGO barrier films with only a slight increase after thermal reduction; 3.66×10^{-5} for both thin and thick GO, and 3.10×10^{-5} for rGO films (values are for plots with time in seconds, Figure 2b, black). This result suggests that the effect of thermal reduction on the diffusivity of the gas through rGO barrier is minimal. More specifically, the nature of permeation paths for rGO remains similar to that of GO (i.e., the diameter and/or the width, and friction between gas species of interests). The slopes for P3HT with Cytop encapsulation and without any encapsulation were 1.93×10^{-4} and 0.20, respectively, giving higher steady-state permeability compared to GO/rGO. In contrast to the minor change observed for steady-state flux, the transition phase shows substantial difference between GO and rGO (Figure 2b, gray). While lag time (also called break-through time, which can be extracted by extrapolation of the slope to the time axis as shown in Figure 1b) was not present (≈0 h) for both controls and 10 nm GO film but it reached 81.2 h for 20 nm GO film, and 510.2 h for the 15 nm rGO film. Large difference in lag time between the films while exhibiting only minor differences in the diffusivity strongly suggests that extremely long diffusion lengths dominate and play a key role in the permeation process of GO/rGO.

More specifically, lag time is a function of two parameters, diffusivity and diffusion length as indicated in the equation:[1]

$$\text{Lagtime(s)} = l^2(\text{cm}^2)/6\,D(\text{cm}^2\text{s}^{-1}) \quad (1)$$

The diffusivities of oxygen obtained from the slopes in the steady-state regime of P3HT transmittance data were found to be 7.6×10^{-8} cm^2 s^{-1} for 20 nm GO, and 6.4×10^{-8} cm^2 s^{-1} for 15 nm rGO film. For comparison, the diffusivity of Cytop is 4×10^{-7} cm^2 s^{-1}.[29] It is clear that the diffusivity of GO/rGO films is not substantially lower than that of polymers, indicating that it is not the origin of superior gas barrier properties of these materials. The diffusion length can be extracted from Equation (1) using the experimentally obtained diffusivity and lag time values above (Figure 2b). The calculated diffusion length for rGO is 8.40 mm, which is 230% of that of GO (see Supporting Information for details). The results quantitatively support that long diffusion length enabled by stacking of rGO sheets plays a crucial role in its superior gas barrier property.

Examination of the material properties of the GO/rGO films provides further insight into the diffusion barrier mechanism. X-ray photoelectron spectroscopy (XPS) shows that mild annealing of GO at 150 °C leads to a decrease in the oxygen content from 54 at% to 34 at%, most of which can be attributed to the removal of water trapped between the sheets.[30,31] Oxygen functional groups such as hydroxyl and carboxyl remained even for rGO, which could affect the degradation process of the encapsulated P3HT films as well as organic electronic devices as those groups attract moisture (Supporting Information Figure S3). The annealing leads to compaction of the structure as shown in **Figure 3**c. This compaction is also confirmed by atomic force microscopy (AFM) measurements that show that the film thickness after annealing decreases from 20 nm to 15 nm. In addition, the mild annealing does not introduce substantial pinhole like defects that are typically found in fully reduced GO.[32] Instead our high-resolution transmission electron microscopy (HRTEM) results revealed that the initial random oxygen functionalized structure of GO (Figure 3a) is replaced by the presence of small highly crystalline regions shown in Figure 3b. The restoration of hexagonal atomic structure in the form of 2–3 nm nanoislands due to removal of oxygen have beneficial effects on barrier property. These islands decrease the interlayer spacing by removal of oxygen group "bridges" as schematically illustrated in side (Figure 3c) and top view (Figure 3d). Above proposed mechanism rely on

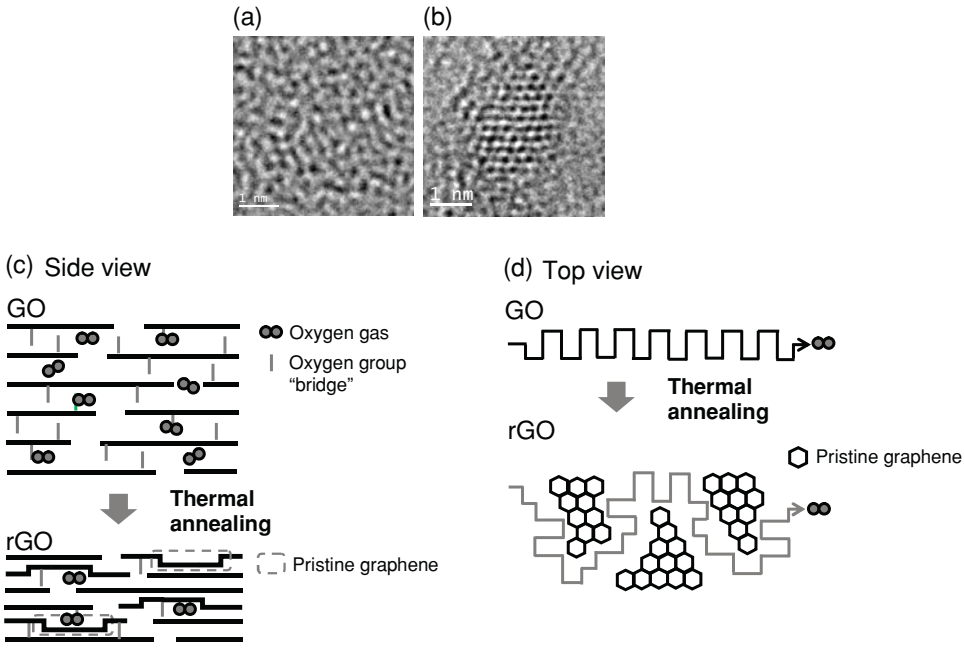

Figure 3. Structural properties of GO/rGO barrier layers. HRTEM image of GO a) before and b) after annealing. Restoration of hexagonal atomic structure in the form of graphene nanoisland can be observed after annealing. Scale bars = 1 nm. c) Schematics of side view showing oxygen gas permeating through GO (top) and rGO (bottom). For the case of GO, oxygen molecules permeates through the interlayer due to presence of oxygen functional groups acting as "bridges". On the other hand, pristine graphene nanoislands created by removal of oxygen group "bridges" clogs permeation paths (dashed boxes), increasing the diffusion length as illustrated in top view (d). Possible permeation paths of the oxygen are indicated by the black and gray arrows for GO and rGO, respectively.

an assumption that AFM and HRTEM results are uniformly distributed over the entire GO/rGO films. Effects of inhomogeneous defects/sheet boundary distrubutions must be taken into account for more accurate permeation mechanisms. It is worthwhile noting water vapor permeates freely through GO (but not rGO).[33] The proposed diffusion mechanism is such that permeated water pillars act as a barrier for gas species. When reduced, removal of oxygen functional groups clogs permeation paths decreasing water permeation to 1/100. It is possible that this is also the case in our system. Assuming that this is the case, our results indicate that oxygen may affect the degradation of P3HT over moisture. Despite the fact that water vapor permeates freely through GO films, their barrier effects were clearly present in the P3HT transmittance test results.

The feasibility of utilizing rGO barriers in real working organic devices was investigated using bulk heterojunction (BHJ) organic solar cells. Specifically, we encapsulated conventional ITO/MoO_3/P3HT:PCBM/Al organic photovoltaic (OPV) devices (**Figure 4**a, see Experimental Section for details). Indium tin oxide (ITO) was on 1 mm thick glass substrate, and the illumination was exposed from bottom of the device through the glass substrate thus optical transmittance of GO and rGO encapsulation films did not affect the device efficiency. The device characteristics were monitored under ambient conditions and under constant illumination, without humidity/moisture control. As shown in current-voltage (I–V) characteristics of the devices for 0 h and 50 h after exposure to ambient conditions (Figure 4b,c, respectively), GO/rGO encapsulation showed clear barrier effect on working organic devices. The absolute power conversion efficiency (PCE) for starting devices ranged between 3.2–3.6% (Supporting Information, Figure S4). The results show that GO/rGO encapsulation improved the normalized PCE by 20% over the period of 50 h (Figure 4d) compared to devices without encapsulation. We found that J_{sc} of the OPVs exhibited substantial changes while FF and V_{oc} remained mostly unchanged. Figure 4e shows the normalized J_{sc} for rGO (circles) and GO encapsulated BHJ solar cells (triangles) compared to control devices (square, without encapsulation). J_{sc} for the device with rGO encapsulation showed less than 5% decrease after 50 h, in contrast to the control devices that show a decrease of nearly 30%. Interestingly, there were no changes in the J_{sc} values for the first 15 h in GO encapsulated devices. This period could be viewed as lag time and it indicates that the lag time of rGO encapsulated devices could be over 50 h. The fluctuation of J_{sc} observed for rGO encapsulated devices in the initial few hours of testing can be attributed to degradation of polymer active layer of the device (P3HT:PCBM blend) induced by the environment (exposure to air and strong illumination), which was also observed as a steeper slope in the initial 5 h of the non-encapsulated device.[34]

3. Conclusion

Solution-processed and optically transparent GO/rGO thin films exhibited improved oxygen/moisture barrier performance over a commercially available Cytop polymer film that has an order of magnitude larger thickness. The barrier performance and lifetime of GO was substantially improved simply by annealing the films at low temperature to obtain rGO. Characterization revealed that the close packing of interlayer distance in addition to restoration of pristine graphene nanoislands induced by

Adv. Energy Mater. **2013**,
DOI: 10.1002/aenm.201300986

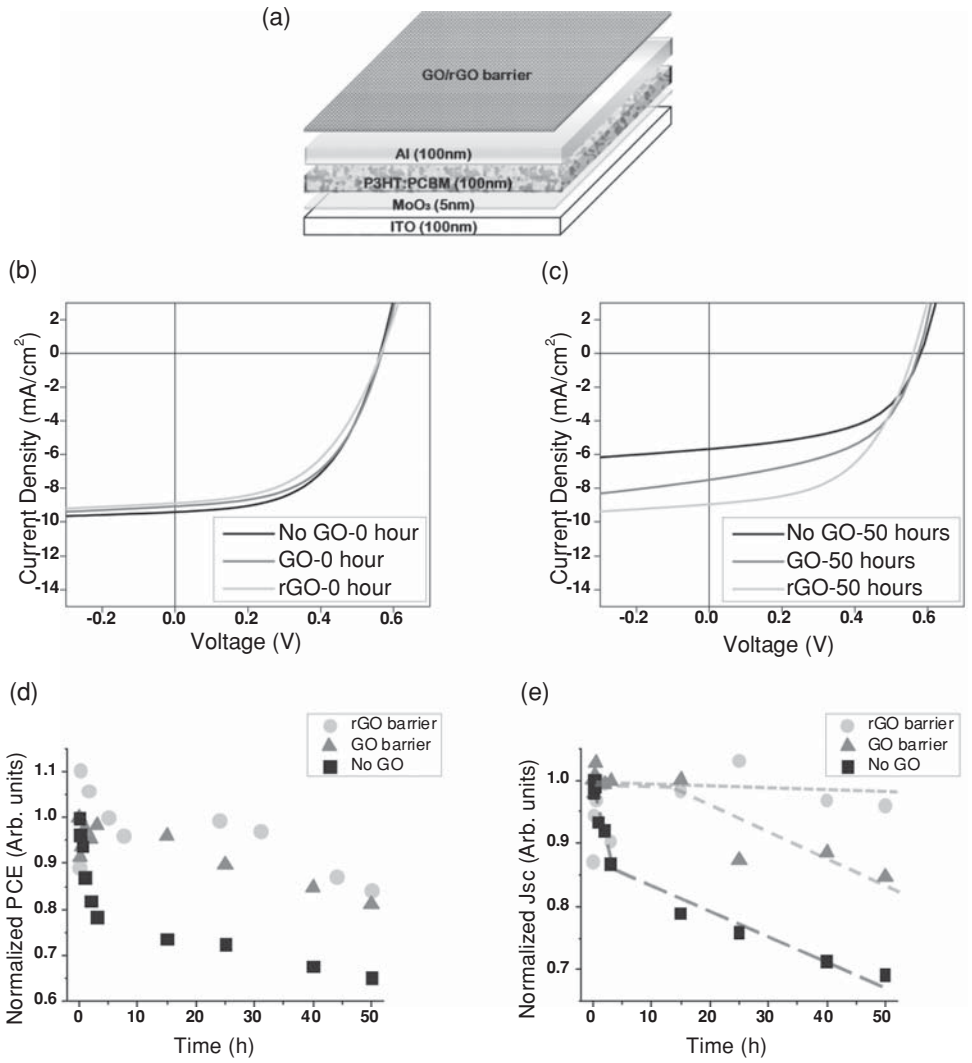

Figure 4. rGO barriers for working organic photovoltaic devices. a) Schematic of the tested device structure. ITO was on 1 mm thick glass substrate, and the illumination was exposed from bottom of the device through the glass substrate. *I–V* characteristics of the devices for b) 0 h and c) 50 h after exposure to ambient conditions. d) Normalized PCE and e) J_{sc} versus tested time of GO/rGO encapsulated BHJ solar cells. Dashed lines are guide for the eye.

the annealing cause clogging of permeation paths, leading to long diffusion lengths, hence long lifetime. The long diffusion length of rGO film was evident from the enhanced lag time. Finally, the gas barrier property of GO/rGO thin films was successfully demonstrated on BHJ solar cells. Our results provide a pathway for realizing high performance and solution processable transparent ultrabarriers that are suitable for wide range of encapsulation applications, including organic electronics.

4. Experimental Section

Sample Preparations and Gas Barrier Measurement Setup: GO was prepared by modified Hummer's method.[18] Briefly, graphite powders were chemically oxidized, exfoliated, and purified by repeated centrifugation. No sonication was applied throughout the process to eliminate formation of pinholes in the GO sheets. Different amount of GO aqueous solution was vacuum filtrated to prepare uniform films of GO with different thicknesses,[18] which were then deposited directly onto the P3HT films for the gas barrier measurements (refer to Figure 1b for the structure of each samples). No post-deposition transfer of the GO films was necessary. Typical film size was 2.54 cm × 2.54 cm (1 inch × 1 inch), with as synthesized films thickness of 10 and 20 nm for thin and thick films, respectively. Some of the 20 nm thick GO films were thermally annealed at 150 °C for 15 min to prepare 15 nm rGO films.

The P3HT transmittance test for gas barrier measurements was performed by using spin-cast P3HT films as oxygen sensors. Organic solvent such as toluene and dichlorobenzene, commonly used for solar cell fabrication was used for dissolving P3HT. The polymer barrier used as a comparison was made by spin-casting a solution of commercially available perfluorinated polymer Cytop to have the thicknesses of >400 nm. An extra care was taken to minimize the light exposure and oxidization of P3HT films during all of the sample preparation procedures. Specifically, the whole processes was performed in the dark to minimize the exposure of P3HT to the light, and P3HT films were always kept in the vacuum desiccators under dark when not in use. The light source of 22 W fluorescent lamp with mean lumens of 783 was used for the test unless stated otherwise. The typical distance between the lamp and the sample surface was ≈5.08 cm (2 inches), where the average power from the lamp was about 0.008 W cm^{-2}. In order to accelerate the testing process, some of the measurements were made using AM 1.5 solar simulator as a light source with power of 100 W cm^{-2} at the sample surface. Transmittance of

P3HT film encapsulated by barrier films are measured and compared with transmittance of reference P3HT (without barrier film) to obtain change in the transmittance of the P3HT films used as sensors.

Material Characterizations: AFM was performed using Digital Instruments Nanoscope IV in tapping mode with standard cantilevers with spring constant of 40 N m^{-1} and tip curvature <10 nm. XPS has been performed with a Thermo Scientific K-Alpha spectrometer equipped with Al Kα microfocused monochromatized source (1486.6 eV), which has an energy resolution of 0.6 eV. Spot size was fixed to 400 µm and the operating pressure was kept at 5×10^{-9} Pa. HRTEM was performed using JOEL JEM-2100F TEM/STEM with double spherical aberration (Cs) correctors (CEOS GmbH, Heidelberg, Germany) to attain high contrast images with a point-to-point resolution of 1.4 Å. The lens aberrations were optimized by evaluating the Zemlin tableau of an amorphous carbon. The residual spherical aberration was almost zero (Cs = –0.8 ± 1.2 µm with 95% certification). The acceleration voltage was set to 120 kV which is the lowest voltage with effective Cs correctors in the system. The region of interests was focused and then recorded with total exposure of less than 20 s (0.5 s exposure time for the image).

Bulk Heterojunction Solar Cell Fabrication and Their Lifetime Tests: Pre-patterned ITO coated glass slides were cleaned thoroughly in distilled water, acetone and isopropyl alcohol by sonication bath for 15 min respectively and dried on a hotplate on 120 °C for 30 min. After being exposed in oxygen plasma for 3 min, a solution of poly(3,4-eth ylenedioxythiophene):poly(styrenesulfonate) (use as purchased, Clevios Al 4083) was spin-coated on top of the ITO slides at 4000 rpm for 40 s resulting in a 40 nm layer. Once the film was dried at 120 °C for 30 min, a blend solution containing 15 mg P3HT (as received from Sigma-Aldrich) and 12 mg [6,6]-phenyl C61 butyric acid methyl ester (PCBM) in 1 mL chlorobenzene was spin-coated at 1500 rpm for 35 s forming approximately 150 nm active layer in argon filled glovebox. Finally, the devices were transferred to vacuum chamber pumped down to 1×10^{-7} Torr for aluminum deposition. The device measurement was carried out in air without humidity/moisture control (relative humidity (RH) of 50–60%), using 100 mW cm^{-2} AM 1.5 solar simulator system calibrated by standard silicon solar cell. The GO/rGO encapsulated and non-encapsulated devices were measured every 10 min for the first 30 min and every few hours afterwards; the devices are stored under room light in air (RH of 50–60%) between each measurement.

Supporting Information

Supporting Information is available from the Wiley Online Library or from the author.

Acknowledgements

The authors acknowledge K. Kuraoka of Kobe University, Japan and G.Eda of National University of Singapore for their technical supports at the initial stage of the work. Authors also acknowledge E. Cheng, J. Kim, and R. Kappera of Rutgers University for the experimental support, D. Watanabe of Tohoku University, Japan for the technical support. H.Y., D.V., M.C. acknowledge Donald H. Jacobs' Chair funding from Rutgers University. H.Y. acknowledges the Japanese Society for the Promotion of Science (JSPS) Postdoctoral Fellowship for Research Abroad, and Laboratory Directed Research and Development (LDRD) Director's Postdoctoral Fellowship of Los Alamos National Laboratory (LANL) for financial support. This research was funded in part by the Center on Materials and Devices for Information Technology Research (CDMITR), the National Science Foundation (NSF) grant #0120967, NSF CMMI 0927736, and Japan Science and Technology Agency (JST), PRESTO.

Received: August 6, 2013
Revised: August 26, 2013
Published online:

[1] G. L. Graff, R. E. Williford, P. E. Burrows, *J. Appl. Phys.* **2004**, *96*, 1840.
[2] J. Meyer, P. Gorrn, F. Bertram, S. Hamwi, T. Winkler, H. H. Johannes, T. Weimann, P. Hinze, T. Riedl, W. Kowalsky, *Adv. Mater.* **2009**, *21*, 1845.
[3] N. Kim, W. J. Potscavage, B. Domercq, B. Kippelen, S. Graham, *Appl. Phys. Lett.* **2009**, 163308.
[4] J. D. Affinito, M. E. Gross, C. A. Coronado, G. L. Graff, E. N. Greenwell, P. M. Martin, *Thin Solid Films* **1996**, *6*, 290.
[5] J. S. Bunch, S. S. Verbridge, J. S. Alden, A. M. van der Zande, J. M. Parpia, H. G. Craighead, P. L. McEuen, *Nano Lett.* **2008**, *8*, 2458.
[6] A. Kolmakov, D. A. Dikin, L. J. Cote, J. Huang, M. K. Abyaneh, M. Amati, L. Gregoratti, S. Günther, M. Kiskinova, *Nat. Nanotechnol.* **2011**, *6*, 651.
[7] S. P. Koenig, L. Wang, J. Pellegrino, J. S. Bunch, *Nat. Nanotechnol.* **2012**, *7*, 728.
[8] K. S. Novoselov, V. I. Falko, L. Colombo, P. R. Gellert, M. G. Schwab, K. Kim, *Nature* **2012**, *490*, 192.
[9] O. Leenaerts, B. Partoens, F. M. Peeters, *Appl. Phys. Lett.* **2008**, *93*, 193105.
[10] S. Chen, L. Brown, M. Levendorf, W. Cai, S.-Y. Ju, J. Edgeworth, X. Li, C. W. Magnuson, A. Velamakanni, R. D. Piner, J. Kang, J. Park, R. S. Ruoff, *ACS Nano* **2011**, 1321.
[11] M. Schriver, W. Regan, W. J. Gannett, A. M. Zaniewski, M. F. Crommie, A. Zettl, *ACS Nano* **2013**, *7*, 5763.
[12] Z. Liu, J. Li, F. Yan, *Adv. Mater.* **2013**, *25*, 4296.
[13] W. S. Hummers, R. E. Offeman, *J. Am. Chem. Soc.* **1958**, *80*, 1339.
[14] M. Hirata, T. Gotou, S. Horiuchi, M. Fujiwara, M. Ohba, *Carbon* **2004**, *42*, 2929.
[15] S. Stankovich, D. A. Dikin, G. H. B. Dommett, K. M. Kohlhaas, E. J. Zimney, E. A. Stach, R. D. Piner, S. T. Nguyen, R. S. Ruoff, *Nature* **2006**, *442*, 282.
[16] G. Eda, M. Chhowalla, *Adv. Mater.* **2010**, *22*, 2392.
[17] A. Bagri, C. Mattevi, M. Acik, Y. J. Chabal, M. Chhowalla, V. B. Shenoy, *Nat. Chem.* **2010**, *2*, 581.
[18] G. Eda, G. Fanchini, M. Chhowalla, *Nat. Nanotechnol.* **2008**, *3*, 270.
[19] J. T. Robinson, M. Zalalutdinov, J. W. Baldwin, E. S. Snow, Z. Wei, P. Sheehan, B. H. Houston, *Nano Lett.* **2008**, *8*, 3441.
[20] H.Yamaguchi, G. Eda, C. Mattevi, H. Kim, M. Chhowalla, *ACS Nano* **2010**, *4*, 524.
[21] O. C. Compton, S. Kim, C. Pierre, J. M. Torkelson, S. T. Nguyen, *Adv. Mater.* **2010**, *22*, 4759.
[22] H. Kim, Y. Miura, C. W. Macosko, *Chem. Mat.* **2010**, *22*, 3441.
[23] Y.-H. Yang, L. Bolling, Morgan A. Priolo, J. C. Grunlan, *Adv. Mater.* **2013**, *25*, 493.
[24] M. Manceau, A. Rivaton, J. L. Gardette, S. Guillerez, N. Lemaitre, *Polym. Degrad. Stabil.* **2009**, *94*, 898.
[25] M. Manceau, S. Chambon, A. Rivaton, J. L. Gardette, S. Guillerez, N. Lemaitre, *Sol. Energy Mater. Sol. Cells* **2010**, *94*, 1572.
[26] L. J. Cote, R. Cruz-Silva, J. Huang, *J. Am. Chem. Soc.* **2009**, *131*, 11027.
[27] J. Granstrom, J. S. Swensen, J. S. Moon, G. Rowell, J. Yuen, A. J. Heeger, *Appl. Phys. Lett.* **2008**, *93*, 193304.
[28] P. Matyba, H. Yamaguchi, M. Chhowalla, N. D. Robinson, L. Edman, *ACS Nano* **2011**, *5*, 574.
[29] Cytop catalog, AGC Chemicals, Asahi Glass Co., Ltd., Tokyo, Japan, January, **2009**.
[30] M. Acik, C. Mattevi, C. Gong, G. Lee, K. Cho, M. Chhowalla, Y. J. Chabal, *ACS Nano* **2010**, *4*, 5861.
[31] C. Mattevi, G. Eda, S. Agnoli, S. Miller, K. A. Mkhoyan, O. Celik, D. Mastrogiovanni, G. Granozzi, E. Garfunkel, M. Chhowalla, *Adv. Funct. Mater.* **2009**, *19*, 2577.
[32] K. Erickson, R. Erni, Z. Lee, N. Alem, W. Gannett, A. Zettl, *Adv Mater.* **2010**, *22*, 4467.
[33] R. R. Nair, H. A. Wu, P. N. Jayaram, I. V. Grigorieva, A. K. Geim, *Science* **2012**, *335*, 442.
[34] C. J. Brabec, S. Gowrisanker, J. J.M. Halls, D. Laird, S. Jia, S. P. Williams, *Adv. Mater.* **2010**, *22*, 3839.